

CEReBrO: Compact Encoder for Representations of Brain Oscillations Using Efficient Alternating Attention

Alexandru Dimofte¹ * Glenn Anta Bucagu¹ Thorir Mar Ingolfsson²

Xiaying Wang² Andrea Cossetti² Luca Benini² Yawei Li² †

¹University of Zurich ²Integrated Systems Laboratory, ETH Zürich, Zürich, Switzerland.

Abstract

Electroencephalograph (EEG) is a crucial tool for studying brain activity. Recently, self-supervised learning methods leveraging large unlabeled datasets have emerged as a potential solution to the scarcity of widely available annotated EEG data. However, current methods suffer from at least one of the following limitations: i) sub-optimal EEG signal modeling, ii) model sizes in the hundreds of millions of trainable parameters, and iii) reliance on private datasets and/or inconsistent public benchmarks, hindering reproducibility. To address these challenges, we introduce a Compact Encoder for Representations of Brain Oscillations using alternating attention (CEReBrO), a new small EEG foundation model. Our tokenization scheme represents EEG signals at a per-channel patch granularity. We propose an alternating attention mechanism that jointly models intra-channel temporal dynamics and inter-channel spatial correlations, achieving 2× speed improvement with 6× less memory required compared to standard self-attention. We present several model sizes ranging from 3.6 million to 85 million parameters. Pre-trained on over 20,000 hours of publicly available scalp EEG recordings with diverse channel configurations, our models set new benchmarks in emotion detection and seizure detection tasks, with competitive performance in anomaly classification and gait prediction. This validates our models' effectiveness.

1. Introduction

An **Electroencephalograph (EEG)** is a fundamental tool for capturing the brain's electrical activity, playing a crucial role in neuroscience research and clinical diagnostics [50]. Its applications are extensive, encompassing disease diagnosis, medical monitoring, and brain-computer interfac-

ing [43]. Modeling EEG signals is inherently challenging due to their non-linear, correlated, and non-stationary nature [40], rendering classical time series models insufficient [5]. The scarcity of annotated EEG data exacerbates these challenges. In fact, high-quality annotations require expert medical professionals, making the process time-consuming, costly, and prone to human error [4, 11, 15, 38]. For example, prolonged monitoring is crucial for conditions like epilepsy, which require continuous tracking over several days, adding to the burden on annotating experts. Furthermore, artifacts such as ocular, cardiac, and muscular activities can mimic seizure patterns and often lead to false alarms and misinterpretations [35, 44, 49].

To address the limited availability of labeled data, self-supervised representation learning methods, *i.e.*, EEG foundation models, have emerged (see Sec. 2). These foundation models are pre-trained on large corpora of unlabeled EEG signals and can generalize to various downstream tasks through fine-tuning. While promising, these models face significant limitations: **1) Sub-optimal balance of spatial and temporal characteristics of EEG signals.**

Self-supervised learning of EEG signals requires a careful balance between the temporal and spatial characteristics of EEG signals, especially in heterogeneous pre-training corpora with varying channel configurations. Some current models either ignore inter-channel spatial interactions [7, 52] or only consider auto-regressive temporal dynamics [8]. Other models strike a better balance between spatial and temporal characteristic modeling, but they either require multi-stage pre-training [21] and/or architectures with hundreds of millions of trainable parameters [56]. **2) Increasing Model Sizes.** The trend toward *Large EEG Foundation Models (LEFMs)*, some exceeding hundreds of millions of parameters [21, 55, 56], raises concerns about computational efficiency and practicality. Without established scaling laws for LEFMs [24], it is unclear if performance gains are due to model component design or model size. This is particularly problematic for real-time applications and deployment on resource-constrained devices like wearable EEG systems [20]. Developing a **Small EEG Founda-**

*Glenn Anta Bucagu and Alexandru Dimofte contributed equally to this work.

†Correspondence to yawli@iis.ee.ethz.ch.

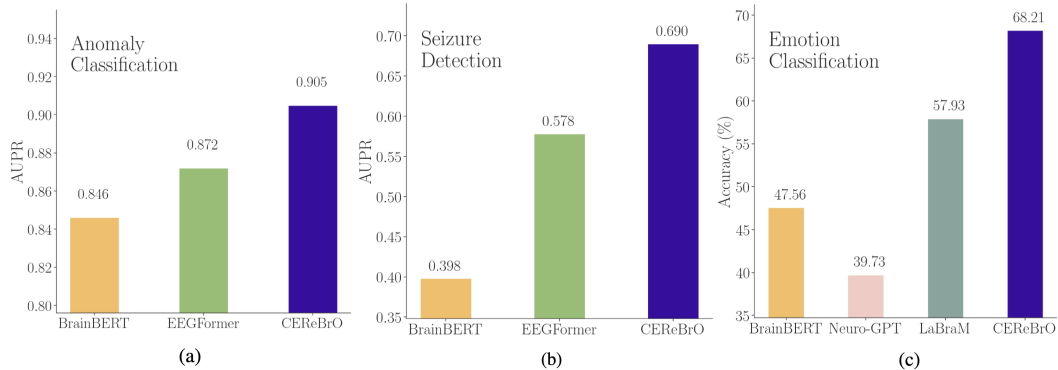


Figure 1. Comparison of CEReBrO with current SOTA in a) anomaly classification, b) seizure detection and c) emotion classification.

tion Model (SEFM) addresses these issues by enabling efficient, real-time processing suitable for widespread deployment. Without a universally accepted definition of SEFMs, we let edge device capabilities dictate our model sizes. The upper limit of tens of millions of trainable parameters is set by the latest smartphones [32, 42] and edge TPU accelerators [41].

3) Data Inconsistency and Privacy. The reliance on private datasets hinders reproducibility and standard benchmarking. Current methods vary in their use of private and public datasets for pre-training and fine-tuning. While some methods [7, 8] exclusively use public datasets, they measure downstream performance on different benchmarks. This complicates comparisons across different models.

Given these challenges, there is a pressing need for efficient EEG models that can handle complex signal dynamics, are suitable for deployment on limited hardware, and promote reproducibility through the use of public datasets. To overcome these limitations we introduce **Compact Encoder for Representations of Brain Oscillations using efficient alternating attention (CEReBrO)**, a SEFM featuring a novel tokenization scheme and an alternating attention mechanism. By alternating between modeling temporal dynamics within individual channels and spatial correlations across different channels, our method effectively captures the complex structure of EEG signals in a single encoder, accommodating diverse channel configurations found in different EEG devices. Our experiments show that this yields significant memory and runtime reductions with improvements in downstream tasks compared to standard self-attention. We pre-train CEReBrO in three sizes (3.6M, 40M, and 85M parameters), drawing inspiration from **Small Language Models (SLMs)** [22, 32, 34] to balance performance and efficiency. Utilizing the **Temple University EEG Corpus (TUEG)** [37] for pre-training ensures reproducibility and facilitates standardized benchmarking. Comprehensive evaluations on public datasets demonstrate CEReBrO’s superior performance and generalizability. These efficiency gains make CEReBrO particularly suitable for deployment

on resource-constrained devices, facilitating real-time EEG analysis in wearable technology.

Our contributions are as follows:

- **Novel Alternating Attention Mechanism:** We propose an efficient method for multi-channel EEG modeling that captures both temporal and spatial information, leading to significant memory reductions (up to $6\times$) and runtime reductions (up to $2\times$) compared to standard self-attention.
- **Development of CEReBrO:** We introduce a compact SEFM that achieves competitive performance with significantly fewer parameters, making it suitable for deployment on resource-constrained devices and facilitating real-time EEG analysis.
- **Large-scale pre-training on TUEG:** We leverage over 20,000 hours of public EEG recordings from more than 10,000 unique subjects, encompassing diverse channel configurations, to ensure robustness and generalizability. To our knowledge, our method is the first to use token padding in pre-training to accommodate different channel configurations in TUEG.
- **Comprehensive Evaluations:** We validate CEReBrO on multiple public benchmarks including anomaly classification, seizure detection, emotion recognition, gait prediction and achieve state-of-the-art performance.

2. Related Works

EEG Foundation Models Recent advancements in EEG foundation models have leveraged Transformer architectures and self-supervised learning techniques to address the scarcity of labeled EEG data. These models aim to learn robust representations from raw EEG signals, facilitating various downstream tasks without extensive labeled datasets.

BENDR [26] is inspired by wav2vec [1] and employs a stack of short-receptive-field 1D convolutions to transform raw EEG waveforms into a sequence of embeddings, which are fed to a Transformer encoder with linear attention modules. Pre-training is done via a contrastive learning objective. However, without explicit channel-specific em-

beddings, BENDR may not optimally differentiate between channels, especially when the number of channels varies between training examples.

BrainBERT [52] uses [Intracranial Electroencephalograph \(iEEG\)](#) spectrogram patches as input tokens to a standard Transformer encoder model, pre-trained via [Masked Autoencoding \(MAE\)](#). By processing channels individually, BrainBERT fails to capture inter-channel correlations, missing crucial spatial relationships inherent in multi-channel EEG data.

LaBraM [21] introduces a learned neural tokenizer that maps patches of EEG waveforms to discrete codebook embeddings, which are then processed by a Transformer encoder within a symmetric MAE framework. The primary limitation of LaBraM is the additional computational overhead required to train the neural tokenizer. Similarly, EEGFormer [7] incorporates a vector quantizer within a Transformer-based model trained via autoencoding, adding complexity to the training process.

Neuro-GPT [8] adapts causal auto-regressive MAE for EEG waveform modeling. In this model, each token aggregates information from multiple channels, limiting the attention mechanism’s ability to balance spatio-temporal characteristics. Neuro-GPT standardizes to 22 channels via nearest neighbor interpolation, which can degrade performance by losing detail from high channel counts and introducing artifacts when interpolating from fewer channels.

Vision Foundation Models We draw on vision foundation models, especially Transformers and self-supervised learning, to enhance EEG signal modeling.

ChannelViT [3] modifies ViT’s [12] patch projection, creating tokens for each channel-patch pair instead of aggregating channels. We adapt this approach from supervised training with RGB, satellite, and microscopy images to self-supervised learning with multi-channel EEG, combining it with alternating attention to capture both temporal and spatial dynamics.

SimMIM [53] and ViTMAE [16] offer distinct self-supervised learning approaches for vision models. SimMIM masks random tokens and processes all tokens through a Transformer encoder, using a linear layer for reconstruction. ViTMAE employs an encoder-decoder architecture, processing only visible tokens in the encoder and reconstructing the input in the decoder. Both optimize masked patch reconstruction. We adapt these MAE styles for EEG, extending the loss function to better capture EEG characteristics.

Our approach addresses limitations in existing EEG foundation models by adapting vision model tokenization and masked image modeling. In addition, we introduce alternating attention, efficiently capturing temporal and spatial dynamics across diverse channel configurations while

reducing computational demands for resource-constrained deployment.

3. Methodology

3.1. Pipeline Overview

In this section, we present **CEReBrO**, a novel [SEFM](#) designed to model EEG waveforms using a compact encoder-only architecture efficiently. We introduce a novel tokenization scheme where EEG waveforms are segmented into patches on a per-channel basis, allowing for granular modeling of temporal dynamics within each channel. This approach uniquely captures both intra-channel and inter-channel correlations, a technique not previously applied to EEG signals to our knowledge. Our encoder consists of Transformer encoder blocks with a novel alternating attention mechanism. Alternating attention facilitates joint modeling of intra-channel temporal dynamics and inter-channel spatial correlations. During pre-training, we randomly mask input tokens. The encoder is optimized by reconstructing the original signals. Key innovations of our pipeline are discussed below.

3.2. Tokenization

Following current literature [36], we slice EEG waveforms into equally-sized non-overlapping patches to: i) enhance the locality and extract semantic information, ii) reduce computation and memory usage, iii) and attend to longer temporal dependencies.

Given an EEG waveform $\mathbf{X} \in \mathbb{R}^{T \times C}$, where T is the number of timestamps and C is the number of channels, we segment \mathbf{X} into non-overlapping patches of length L with stride S . This results in a set of patches $\mathbf{P} \in \mathbb{R}^{N_p \times C \times L}$, where $N_p = \lfloor \frac{T-L}{S} + 1 \rfloor$ is the number of patches per channel. Each patch $\mathbf{P}_{c,i} \in \mathbb{R}^L$ from channel c and patch index i is projected onto an embedding space of dimension d_e using a learnable linear projection $\mathbf{W}_{\text{proj}} \in \mathbb{R}^{d_e \times L}$. The embedded patches are given by $\mathbf{E}_{c,i} = \mathbf{W}_{\text{proj}} \mathbf{P}_{c,i}^T$. We then add learnable positional embeddings $\mathbf{W}_{\text{pos}} \in \mathbb{R}^{N_p \times d_e}$ and channel embeddings $\mathbf{W}_{\text{chan}} \in \mathbb{R}^{C \times d_e}$. The input embeddings are calculated as:

$$\mathbf{E}_{c,i}^{\text{in}} = \mathbf{E}_{c,i} + \mathbf{W}_{\text{pos},i} + \mathbf{W}_{\text{chan},c}$$

where $\mathbf{W}_{\text{pos},i} \in \mathbb{R}^{d_e}$ is the positional embedding for patch index i , and $\mathbf{W}_{\text{chan},c} \in \mathbb{R}^{d_e}$ is the channel embedding for channel c . This per-channel patch granularity of our tokens allows us to model intra-channel and inter-channel correlations jointly.

3.3. Model Architecture

We use a Transformer encoder model [51] with N layers, each comprising H attention heads and embedding dimension d_e . Due to the fine-grained tokenization, each training

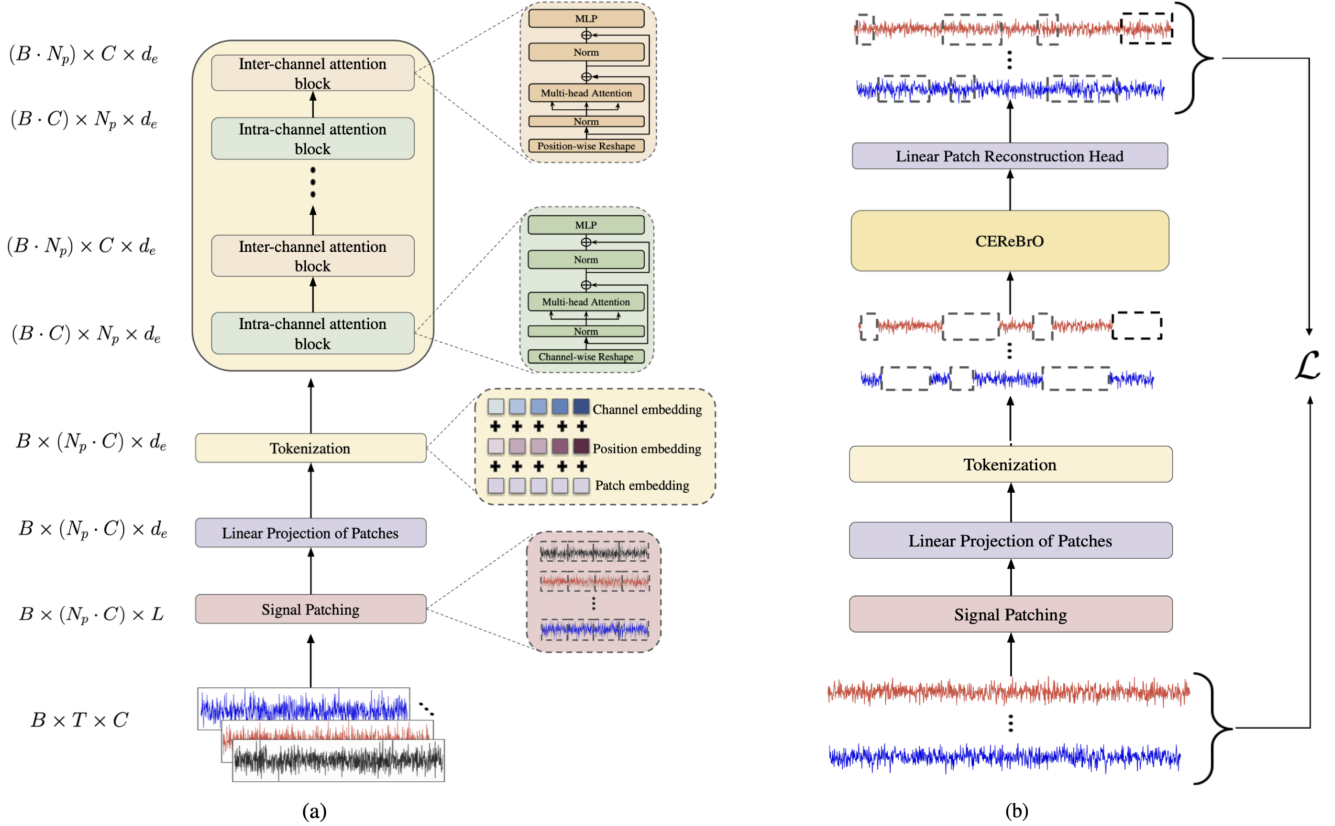


Figure 2. (a) Overview of the CEReBrO architecture. (b) Overview of our pre-training framework.

example can contain up to several thousand tokens, increasing the computation complexity of the self-attention mechanism that scales quadratically with sequence length. To address this, we introduce an alternating attention mechanism (Algorithm 1) within the Transformer encoder. This mechanism alternates between intra-channel and inter-channel attention in successive layers.

In intra-channel attention layers, we focus on temporal dependencies within each channel by computing attention over the sequence of patches in that channel. In inter-channel attention layers, we capture spatial correlations by computing attention across channels at each time step. We use an even number of encoder layers so that both intra-channel and inter-channel attention are equally represented. The inputs to the first layer are the previously introduced input embeddings $\mathbf{E}_{c,i}^{\text{in}}$. Each layer alternates between intra-channel and inter-channel multi-head attention, applies a feed-forward network, and is followed by layer normalization. The outputs $\mathbf{E}_{c,i}^{(j)}$ of the j -th layer serve as the inputs to the $(j + 1)$ -th layer.

During both pre-training and fine-tuning, the output of the final encoder layer is passed to a single linear layer. In pre-training, this linear layer serves as a patch reconstruction head; in fine-tuning, it functions as a classification

layer. Our alternating attention mechanism is notable for two reasons: i) it allows us to jointly model intra-channel temporal dynamics and inter-channel spatial correlations within a single encoder, and ii) it enables efficient attention computation over long EEG token sequences. We illustrate our end-to-end pipeline in Fig. 2.

3.4. Theoretical and Empirical Analysis of Alternating Attention

For standard self-attention, the memory complexity is quadratic with respect to sequence length because the attention mechanism considers pairwise interactions between all tokens in the sequence. In our alternating attention mechanism, the memory complexity alternates between:

- **intra-channel attention** layers, where attention is computed within each channel independently over N_p patches, resulting in a total complexity of $\mathcal{O}(CN_p^2)$.
- **inter-channel attention** layers, where attention is computed across C channels at each of the N_p time steps, resulting in a complexity of $\mathcal{O}(C^2N_p)$.

Overall, the alternating attention mechanism significantly reduces the memory and computational requirements compared to standard self-attention, mainly when C and N_p are large. This reduction enables efficient processing of long EEG sequences and high-channel-count data.

Algorithm 1 ALTERNATING ATTENTION MECHANISM

Require: Input tensor \mathbf{T} of shape $[B, C \times N_p, d_e]$

Parameters:

B : batch size

C : number of channels

N_p : number of patches per channel

d_e : embedding dimension

```
1: for each encoder layer  $i$  to  $N$  do
2:   if  $i$  is odd then ▷ Inter-channel attention
3:     Reshape  $\mathbf{T}$  to  $[B \times N_p, C, d_e]$ 
4:     Compute QKV projection
5:     Multi-head attention over  $C$  (channels)
6:   else ▷ Intra-channel attention
7:     Reshape  $\mathbf{T}$  to  $[B \times C, N_p, d_e]$ 
8:     Compute QKV projection
9:     Multi-head attention over  $N_p$  (patches)
10:  end if
11:  Reshape output back to  $[B, C \times N_p, d_e]$ 
12: end for
```

Ensure: Output tensor of shape $[B, C \times N_p, d_e]$

Attention Type	Memory Complexity	Time Complexity
Intra-channel	$\mathcal{O}(CN_p^2)$	$\mathcal{O}(CN_p^2d_e)$
Inter-channel	$\mathcal{O}(C^2N_p)$	$\mathcal{O}(C^2N_pd_e)$
Standard Self-Attention	$\mathcal{O}((CN_p)^2)$	$\mathcal{O}((CN_p)^2d_e)$

Table 1. Theoretical memory and time complexities of each attention type.

We empirically compare alternating attention and standard self-attention by measuring GPU memory requirements and runtime vs. sequence length of the forward pass for three different CEReBrO model sizes. To replicate conditions typically used in state-of-the-art models, we use $N_p = 64$ and $C \in [1, 64]$. Experiments are conducted on 4 NVIDIA RTX 2080 Ti GPUs. In Fig. 6b, we see that for the largest sequence lengths, assuming equal model size, standard self-attention yields $> 2\times$ the runtime compared to alternating attention. In Fig. 3a, assuming equal model size, standard self-attention consumes $> 6\times$ the GPU memory consumed by alternating attention. These results are consistent with our theoretical analysis in Tab. 1. Alternating attention is particularly efficient for large values of CN_p . This includes settings with long EEG signals and/or many EEG channels. More details regarding split attention can be found in Sec. B.

There exist efficient alternatives to self-attention, including low-rank approximation methods [6], linear attention [25] and sparse attention [33] among many others. These methods typically provide memory and/or runtime improvements at the cost of performance compared to standard self-attention. This appears to be true for alternating attention applied to EEG spectrograms. However, we find that al-

ternating attention on EEG waveforms can actually provide performance improvements compared to standard self-attention (see Sec. 4). In theory, alternating attention can be combined with other self-attention alternatives (e.g. low rank approximations, linear attention etc) for potentially greater efficiency. Alternating attention can also, by design, be extended to general multi-channel timeseries and multi-channel images (although performance may vary by task). We leave these explorations for future research.

3.5. Pre-training

We use MAE during pre-training to allow our model to learn useful representations from a large unlabeled pre-training corpus. After patching of EEG waveforms, we randomly mask a fixed portion of patches in each input sequence of patches \mathbf{P} . Masked positions are replaced with a single shared learnable [MASK] token. The resulting sequence of tokens is passed to our Transformer encoder. The encoder output is then passed to a linear layer that outputs a sequence $\hat{\mathbf{P}}$, which is a reconstruction of \mathbf{P} . We define the following loss components:

$$\mathcal{L}_{\text{masked}} = \frac{1}{|\overline{M}|} \sum_{(c,i) \in \overline{M}} \|\mathbf{P}_{c,i} - \hat{\mathbf{P}}_{c,i}\|_2^2 \quad (1)$$

$$\mathcal{L}_{\text{visible}} = \frac{1}{|M|} \sum_{(c,i) \in M} \|\mathbf{P}_{c,i} - \hat{\mathbf{P}}_{c,i}\|_2^2 \quad (2)$$

where M and \overline{M} are the set of masked and visible token positions respectively. Our total loss function during pre-training is:

$$\mathcal{L} = \mathcal{L}_{\text{masked}} + \alpha \mathcal{L}_{\text{visible}} \quad (3)$$

Traditional MAE methods [10, 16, 19, 52, 53] compute the reconstruction loss only on masked patches (i.e., $\alpha = 0$). We observed that doing so with our framework led to high-quality reconstructions of masked patches but relatively poor and unpredictable reconstructions of visible patches. Inspired by findings in [16], which showed that computing the loss uniformly on all tokens (i.e., $\alpha = 1$) can reduce downstream performance, we introduce $\mathcal{L}_{\text{visible}}$ with a small weighting factor $\alpha = 0.1$. This approach stabilizes the reconstruction of visible patches while preventing the model from learning the identity function, thereby enhancing downstream performance. Similar strategies have been employed in lightweight vision transformers [47], demonstrating improved performance on low-resolution image datasets. We illustrate our pre-training framework in Fig. 2.

3.6. Fine-tuning

We use our pre-trained encoder model as a feature extractor for a single linear layer classifier. While most MAE methods use a [CLS] token, we adopt global mean pooling over

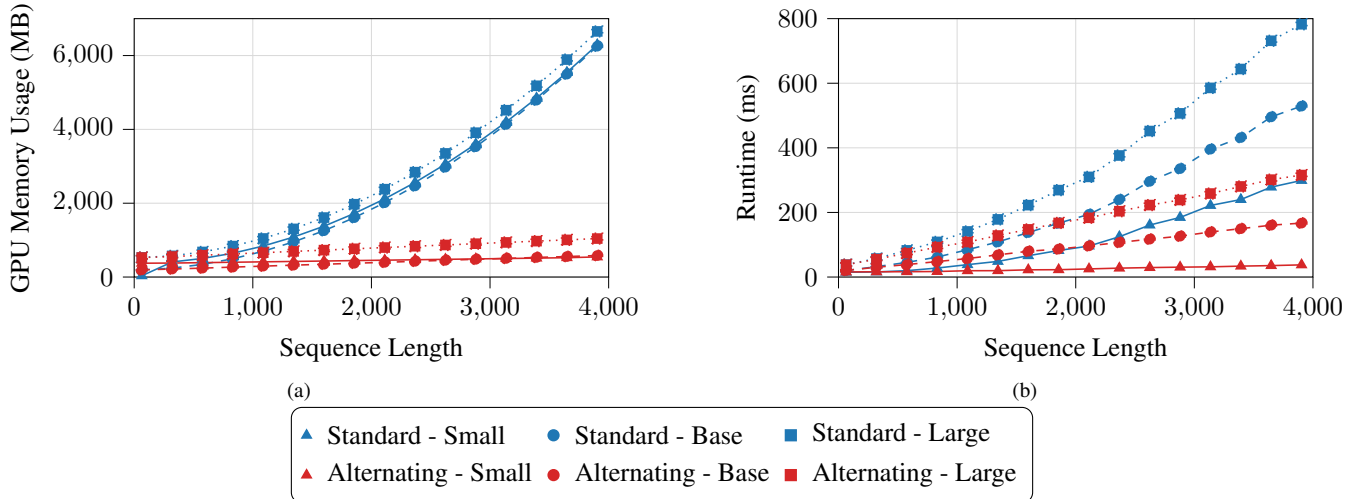


Figure 3. Forward pass GPU Memory Usage (a) and Runtime (b) vs. Sequence Length for alternating attention and standard self-attention in three CEReBrO model sizes. We use $N_p = 20$ and $C \in [1, 64]$ to simulate typical EEG configurations.

the token embeddings to aggregate information. This choice avoids additional computational overhead associated with a [CLS] token, which would require extra processing steps in the alternating attention mechanism framework. Empirically, using mean pooling yields comparable performance to using a [CLS] token [16]. The encoder weights can either be frozen (linear probing) or used as initialization (full fine-tuning). While full fine-tuning requires more computational resources, it generally yields better downstream performance.

3.7. Handling Different Channel Numbers In Pre-training

To handle varying numbers of channels, we pad the input sequences to a maximum channel count using a shared learnable [PAD] token, taking inspiration from LLMs [10]. This allows the model to process inputs with different channel configurations within a unified architecture. The attention scores corresponding to [PAD] tokens are forced to zero during attention computations to prevent them from influencing the model’s output. While padding increases the input sequence length, we limit the maximum number of channels to a reasonable upper bound (e.g. 64 channels) to control computational costs. This limit on the number of channels (and hence the context length of our model) justifies why padding is a reasonable mechanism for our specific case, as EEG recording devices have a practical maximum number of channels due to physical constraints [13].

4. Experiments

4.1. Data

We pre-train our model on TUEG [37]. This totals over 20,000 hours of EEG signals from over 10,000 unique sub-

jects and a wide variety of EEG channel configurations (18-36 channels). This is the largest publicly available scalp EEG corpus in the world and it covers an expansive range of pathologies and neural signals. We evaluate our model on several downstream tasks described by the following datasets:

- i. TUAB [37]: EEG recordings (23 channels sampled at 250 Hz) from 2,329 subjects with normal/abnormal annotations.
- ii. SEED [57]: EEG recordings (62 channels sampled at 200 Hz) from 15 subjects with annotations negative/neutral/positive emotion annotations in response to various movie clips.
- iii. Neonate [46]: EEG recordings (19 channels sampled at 250 Hz) with annotated seizures for 79 Neonates.

All our pre-training and downstream data is publicly available, which we believe will facilitate benchmarking and development of EEG foundation models. More details regarding our dataset pre-processing are available in Sec. A.

4.2. EEG Representation and Pre-training Style

We compare pre-training and fine-tuning with waveforms and spectrograms. While waveforms purely provide time information, spectrograms are a popular representation method in LEFMs [52] since they strike a balance between time and frequency resolution [14]. Following [52], we compute spectrogram representations using the Short-Time Fourier Transform. We also compare SimMIM and ViTMAE pre-training styles. While SimMIM uses a single-encoder only pre-training, ViTMAE separates pre-training into an encoder and lightweight Transformer decoder. In this setting, the encoder only provides representations of visible tokens and the decoder uses encoder outputs and masked tokens to reconstruct signals. For each candidate

model, we fine-tune on TUAB and report balanced accuracy, macro AUPR and macro AUROC scores. We choose TUAB as our performance proxy because of its popularity in EEG Foundation Model literature. To illustrate the importance of pre-training, we also show model performance when trained from scratch directly on TUAB. Our results are summarized in Tab. 2. More experiments on spectrograms can be found in Sec. C.

Representation	Pre-training Style	Balanced Accuracy (%)	AUPR	AUROC
Spectrograms	None	76.49	0.8462	0.8483
	ViTMAE	77.71	0.8586	0.8559
	SimMIM	78.33	0.8659	0.8595
Waveforms	None	76.39	0.8430	0.8426
	SimMIM	79.35	0.8755	0.8700
	ViTMAE	79.42	0.8741	0.8715

Table 2. Comparing EEG signal representation and pre-training style.

From Tab. 2, we observe that pre-training significantly improves performance over training from scratch, with waveform representations slightly outperforming spectrograms in our setting. This suggests that preserving temporal information in raw waveforms may be more beneficial for certain EEG tasks, possibly due to the loss of fine-grained temporal details in spectrograms. The performance gains, although modest compared to the amount of pre-training data used, align with observations in other works [16, 53], indicating diminishing returns with large-scale pre-training. Comparing pre-training styles, SimMIM and ViTMAE yield similar performance, with SimMIM being slightly better for spectrograms and ViTMAE for waveforms. This may be attributed to the inherent differences in how each method handles masked tokens and reconstruction objectives, affecting their ability to capture relevant features in different representations.

4.3. Spectrogram Patching

Spectrograms can be patched in different ways. Square patches are typically used in vision foundation models [16, 53]. Time bin patches have also been proposed specifically for spectrogram-related tasks [19, 52]. We illustrate the difference in Fig. 4.

We compare the use of square patches and time bin patches in spectrogram tokenization. Note that this also means we are comparing random unstructured masking with time bin masking. Results are outlined in Tab. 3.

In Tab. 3, we observe that time bin patching yields better downstream performance on TUAB compared to the classical square patching. Time bin patching is both superior in the training from scratch and pre-trained regimes. We posit that this is partly due to the natural sequential nature of tokens when time bin patching is used.

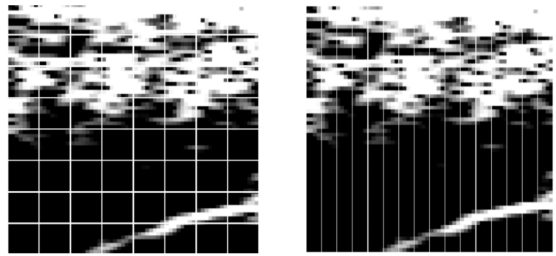


Figure 4. Spectrogram square patching (left) and time bin patching (right)

Patching	Pre-training Style	Balanced Accuracy (%)	AUPR	AUROC
Square patches	None	76.49	0.8462	0.8483
Time bin patches	None	77.24	0.8489	0.8498
Square patches	SimMIM	78.33	0.8659	0.8595
Time bin patches	SimMIM	78.89	0.8719	0.8690

Table 3. The effect of patch shape and masking strategy on downstream performance.

4.4. Alternating Attention vs. Standard Attention

We aim to evaluate the impact of the alternating attention mechanism on downstream performance compared to using standard self-attention. Using the best-performing waveform and spectrogram models identified in Sec. 4.2, we compare the two attention mechanisms. We focus on the SimMIM pre-training style, as the ViTMAE style benefits less from alternating attention due to its use of only visible tokens in the encoder. Our results are presented in Tab. 4.

Representation	Attention	Balanced Accuracy (%)	AUPR	AUROC
Spectrogram	Alternating	78.49	0.8684	0.8674
	Self-Attention	78.89	0.8719	0.8690
Waveform	Self-Attention	79.35	0.8755	0.8700
	Alternating	80.65	0.8901	0.8825

Table 4. Comparing standard self-attention and alternating attention.

From Tab. 4, we observe differing outcomes between spectrograms and waveform representations. For spectrograms, standard self-attention marginally outperforms alternating attention across all performance metrics. This may be due to spectrograms already encapsulating frequency and temporal information in a two-dimensional format, where global attention can effectively capture relevant features.

In contrast, for waveforms, alternating attention significantly outperforms standard self-attention, achieving improvements of +1.3% in balanced accuracy, +0.0146 in AUPR and +0.0125 AUROC. This suggests that the alternating attention mechanism is more adept at capturing the inherent temporal dynamics and spatial correlations in raw waveforms, likely because it explicitly models intra-

channel and inter-channel relationships. These results indicate that alternating attention is particularly beneficial when dealing with raw waveform data, emphasizing its suitability for modeling EEG signals in their original temporal form.

4.5. Comparisons with the State of the Art

We validate our model architecture and demonstrate its effectiveness in learning meaningful representations that generalize across various downstream tasks, including anomaly classification, emotion recognition and seizure detection¹. Details regarding our experimental setup are in Sec. A. We provide results on gait prediction in Sec. D.

Method	Model Size	Accuracy (%)	F1
Supervised Models			
LSTM [18]	-	44.31	0.4277
ConvNeXt [31]	3.7M	52.50	0.5155
Self-supervised Models			
BrainBERT [52]	43.18M	47.56	0.4679
Neuro-GPT [8]	79.53M	39.73	0.3949
LaBraM [21]	46M	57.93	0.5899
CEReBrO	3.58M	54.57 ± 0.56	0.5475 ± 0.0058
CEReBrO	39.95M	67.18 ± 0.24	0.6732 ± 0.0023
CEReBrO	85.15M	68.21 ± 0.63	0.6845 ± 0.0061

Table 5. Performance on emotion classification using SEED.

Tab. 5 compares our approach to state-of-the-art emotion classification. Among the supervised methods, ConvNeXt achieves the highest performance while using 3.5M parameters. In comparison, BrainBERT and Neuro-GPT use more 11× and 21× more parameters respectively, while achieving lower performance. LaBraM remains competitive with +2% accuracy and +0.3 F1 score compared to CEReBrO at a comparable size. At its smallest size, CEReBrO outperforms all supervised approaches despite having less parameters, demonstrating the effectiveness of our method. At its largest size, CEReBrO achieves a new state-of-the-art performance.

Method	Model Size	AUPR	AUROC
Supervised Models			
EEGNet [27]	-	0.499 ± 0.044	0.793 ± 0.019
TCN [2]	-	0.398 ± 0.025	0.731 ± 0.020
EEG-GNN [9]	0.107M	0.419 ± 0.021	0.760 ± 0.010
GraphS4mer [48]	0.266M	0.374 ± 0.013	0.719 ± 0.007
STATENET [30]	-	0.789	0.910
Self-supervised Models			
BrainBERT [52]	43.18M	0.398 ± 0.027	0.734 ± 0.019
EEGFormer Small [7]	-	0.578 ± 0.023	0.842 ± 0.008
EEGFormer Base [7]	-	0.568 ± 0.036	0.842 ± 0.014
EEGFormer Large [7]	-	0.544 ± 0.026	0.833 ± 0.017
CEReBrO	3.58M	0.576 ± 0.089	0.830 ± 0.037
CEReBrO	39.95M	0.676 ± 0.092	0.867 ± 0.039
CEReBrO	85.15M	0.690 ± 0.091	0.875 ± 0.039

Table 6. Performance on seizure detection using the Neonate Seizure dataset

¹All performance metrics are established by existing methods. We are unable to train models other than CEReBrO due to limited resources. "-" indicates missing information not found in publications, lacking open-source implementation, and for which the authors did not respond.

Tab. 6 evaluates CEReBrO in seizure detection. Our smallest model achieves a comparable performance to all variants of EEGFormer. When a larger model is considered (85M), we achieve a much higher AUROC, reaching a maximum value of 0.875. While this number is still lower than the 0.91 from STATENET, CEReBrO sets a new state-of-the-art among foundation models capable of handling different downstream tasks.

Methods	Model Size	Balanced Accuracy (%)	AUPR	AUROC
Supervised Models				
SPaRCNet [23]	0.79M	78.96 ± 0.18	0.8414 ± 0.0018	0.8676 ± 0.0012
CNN-Transformer [39]	3.2M	77.77 ± 0.22	0.8433 ± 0.0039	0.8461 ± 0.0013
FFCL [28]	2.4M	78.48 ± 0.38	0.8448 ± 0.0065	0.8569 ± 0.0051
ST-Transformer [45]	3.5M	79.66 ± 0.23	0.8521 ± 0.0026	0.8707 ± 0.0019
Self-supervised Models				
BrainBERT [52]	43.18M	-	0.8460 ± 0.0030	0.8530 ± 0.0020
EEGFormer Small [7]	-	-	0.8620 ± 0.0050	0.8620 ± 0.0070
EEGFormer Base [7]	-	-	0.8670 ± 0.0020	0.8650 ± 0.0010
EEGFormer Large [7]	-	-	0.8720 ± 0.0010	0.8760 ± 0.0030
LaBraM [21]	5.8M	81.40 ± 0.19	0.8965 ± 0.0016	0.9022 ± 0.0009
LaBraM [21]	46M	82.26 ± 0.15	0.9130 ± 0.0005	0.9127 ± 0.0005
LaBraM [21]	369M	82.58 ± 0.11	0.9204 ± 0.0011	0.9162 ± 0.0016
CEReBrO	3.58 M	79.40 ± 0.19	0.8763 ± 0.0031	0.8749 ± 0.0033
CEReBrO	39.95 M	81.29 ± 0.15	0.8994 ± 0.0002	0.8867 ± 0.0006
CEReBrO	85.15 M	81.67 ± 0.23	0.9049 ± 0.0026	0.8916 ± 0.0038

Table 7. Performance on anomaly classification using TUAB.

Finally, Tab. 7 compares the performance of our approach to state-of-the-art in anomaly classification tasks. Among the supervised models, ST-Transformer achieves the highest accuracy (79.66%) with a model size of 3.5M. LaBraM surpasses ST-Transformer in accuracy by approx. +2% when keeping a comparable model size and by +3% when considering a much larger model (369M). In comparison, CEReBrO achieves a performance comparable to ST-Transformer at a similar model size. Furthermore, we achieve a maximum accuracy comparable to LaBraM with a model size up to 4× smaller. A detailed comparison of LaBraM and CEReBrO can be found in Sec. E.

5. Conclusion

We propose CEReBrO, a compact encoder-only model with a novel alternating attention mechanism. Our model efficiently captures the spatio-temporal characteristics of EEG signals. For 3 model sizes between 3.6 million and 85 million parameters, alternating attention achieves 2× the speed improvements and consumes 6× less memory than standard self-attention especially for long input sequences. CEReBrO is pre-trained on public heterogeneous EEG signals and displays impressive performance on public downstream benchmarks, often matching or surpassing larger and more resource-intensive methods. Although EEG foundation models have not yet reached the scale of modern Large Language Models (LLMs), there is substantial potential in developing smaller, more efficient architectures tailored to EEG data.

6. Acknowledgements

This work was supported by the ETH Future Computing Laboratory (EFCL), financed by a donation from Huawei Technologies. This work was supported by a grant from the Swiss National Supercomputing Centre (CSCS) under project ID lp12 on Alps.

References

- [1] Alexei Baevski, Henry Zhou, Abdelrahman Mohamed, and Michael Auli. wav2vec 2.0: A framework for self-supervised learning of speech representations. In *Thirty-fourth Conference on Neural Information Processing Systems*, 2020. 2
- [2] Shaojie Bai, J. Zico Kolter, and Vladlen Koltun. An empirical evaluation of generic convolutional and recurrent networks for sequence modeling, 2018. 8
- [3] Yujia Bao, Srinivasan Sivanandan, and Theofanis Karaletsos. Channel vision transformers: An image is worth $1 \times 16 \times 16$ words. In *The Twelfth International Conference on Learning Representations*, 2024. 3
- [4] Megan A. Boudewyn, Molly A. Erickson, Kurt Winsler, John Daniel Ragland, Andrew Yonelinas, Michael Frank, Steven M. Silverstein, Jim Gold, Angus W. 3rd MacDonald, Cameron S. Carter, Deanna M. Barch, and Steven J. Luck. Managing EEG studies: How to prepare and what to do once data collection has begun. *Psychophysiology*, 60(11):e14365, 2023. 1
- [5] Peter J. Brockwell and Richard A. Davis. *Introduction to Time Series and Forecasting*. Springer, Cham, 3 edition, 2016. 1
- [6] Beidi Chen, Tri Dao, Eric Winsor, Zhao Song, Atri Rudra, and Christopher Ré. Scatterbrain: Unifying sparse and low-rank attention approximation, 2021. 5
- [7] Yuqi Chen, Kan Ren, Kaitao Song, Yansen Wang, Yifan Wang, Dongsheng Li, and Lili Qiu. Eegformer: Towards transferable and interpretable large-scale eeg foundation model, 2024. 1, 2, 3, 8
- [8] Wenhui Cui, Woojae Jeong, Philipp Thölke, Takfarinas Medani, Karim Jerbi, Anand A. Joshi, and Richard M. Leahy. Neuro-gpt: Towards a foundation model for eeg, 2024. 1, 2, 3, 8
- [9] Andac Demir, Toshiaki Koike-Akino, Ye Wang, Masaki Haruna, and Deniz Erdogmus. Eeg-gnn: Graph neural networks for classification of electroencephalogram (eeg) signals, 2021. 8
- [10] Jacob Devlin, Ming-Wei Chang, Kenton Lee, and Kristina Toutanova. Bert: Pre-training of deep bidirectional transformers for language understanding, 2019. 5, 6
- [11] Marina Diachenko, Simon J. Houtman, Erika L. Juarez-Martinez, Jennifer R. Ramautar, Roos Weiler, Huibert D. Mansvelder, Hilgo Bruining, Peter Bloem, and Klaus Linkenkaer-Hansen. Improved manual annotation of EEG signals through convolutional neural network guidance. *eNeuro*, 9(5):ENEURO.0160–22.2022, 2022. 1
- [12] Alexey Dosovitskiy, Lucas Beyer, Alexander Kolesnikov, Dirk Weissenborn, Xiaohua Zhai, Thomas Unterthiner, Mostafa Dehghani, Matthias Minderer, Georg Heigold, Sylvain Gelly, Jakob Uszkoreit, and Neil Houlsby. An image is worth 16×16 words: Transformers for image recognition at scale. In *International Conference on Learning Representations*, 2021. 3
- [13] Electrical Geodesics, Inc. The geodesic sensor net, 2024. Accessed on November 01, 2024. 6
- [14] Hans G. Feichtinger and Thomas Strohmer, editors. *Gabor Analysis and Algorithms*. Birkhäuser, Boston, MA, 1998. 6
- [15] Bharat Gurnani and Kirandeep Kaur. Data annotators: The unclaimed heroes of artificial intelligence revolution in ophthalmology. *Indian Journal of Ophthalmology*, 70(5):1847, 2022. 1
- [16] Kaiming He, Xinlei Chen, Saining Xie, Yanghao Li, Piotr Dollár, and Ross Girshick. Masked autoencoders are scalable vision learners, 2021. 3, 5, 6, 7
- [17] Yongjie He, Tuan Luu, Karunesh Nathan, et al. A mobile brain-body imaging dataset recorded during treadmill walking with a brain-computer interface. *Scientific Data*, 5:180074, 2018. 15
- [18] Sepp Hochreiter and Jürgen Schmidhuber. Long short-term memory. *Neural Computation*, 9(8):1735–1780, 1997. 8
- [19] Po-Yao Huang, Hu Xu, Juncheng B Li, Alexei Baevski, Michael Auli, Wojciech Galuba, Florian Metze, and Christoph Feichtenhofer. Masked autoencoders that listen. In *Advances in Neural Information Processing Systems*, 2022. 5, 7
- [20] Thorir Mar Ingólfsson, Xiaying Wang, Upasana Chakraborty, Simone Benatti, Adriano Bernini, Pauline Ducouret, Philippe Ryvlin, Sandor Beniczky, Luca Benini, and Andrea Cossettini. Brainfusenet: Enhancing wearable seizure detection through eeg-ppg-accelerometer sensor fusion and efficient edge deployment. *IEEE Transactions on Biomedical Circuits and Systems*, 2024. 1
- [21] Weibang Jiang, Liming Zhao, and Bao liang Lu. Large brain model for learning generic representations with tremendous EEG data in BCI. In *The Twelfth International Conference on Learning Representations*, 2024. 1, 3, 8, 15
- [22] Xiaoqi Jiao, Yichun Yin, Lifeng Shang, Xin Jiang, Xiao Chen, Linlin Li, Fang Wang, and Qun Liu. Tinybert: Distilling bert for natural language understanding, 2020. 2
- [23] J. Jing, W. Ge, S. Hong, M. B. Fernandes, Z. Lin, C. Yang, S. An, A. F. Struck, A. Herlopian, I. Karakis, J. J. Halford, M. C. Ng, E. L. Johnson, B. L. Appavu, R. A. Sarkis, G. Osman, P. W. Kaplan, M. B. Dhakar, L. Arcot Jayagopal, Z. Sheikh, O. Taraschenko, S. Schmitt, H. A. Haider, J. A. Kim, C. B. Swisher, N. Gaspard, M. C. Cervenka, A. A. Rodriguez Ruiz, J. W. Lee, M. Tabaeizadeh, E. J. Gilmore, K. Nordstrom, J. Y. Yoo, M. G. Holmes, S. T. Herman, J. A. Williams, J. Pathmanathan, F. A. Nascimento, Z. Fan, S. Nasiri, M. M. Shafi, S. S. Cash, D. B. Hoch, A. J. Cole, E. S. Rosenthal, S. F. Zafar, J. Sun, and M. B. Westover. Development of expert-level classification of seizures and rhythmic and periodic patterns during eeg interpretation. *Neurology*, 100(17):e1750–e1762, 2023. PMID: 36878708; PMCID: PMC10136013. 8, 15
- [24] Jared Kaplan, Sam McCandlish, Tom Henighan, Tom B. Brown, Benjamin Chess, Rewon Child, Scott Gray, Alec

- Radford, Jeffrey Wu, and Dario Amodei. Scaling laws for neural language models, 2020. 1
- [25] Angelos Katharopoulos, Apoorv Vyas, Nikolaos Pappas, and François Fleuret. Transformers are rnns: Fast autoregressive transformers with linear attention, 2020. 5
- [26] Demetres Kostas, Stephane Aroca-Ouellette, and Frank Rudzicz. Bendr: using transformers and a contrastive self-supervised learning task to learn from massive amounts of eeg data, 2021. 2
- [27] Vernon J Lawhern, Amelia J Solon, Nicholas R Waytowich, Stephen M Gordon, Chou P Hung, and Brent J Lance. Eegnet: a compact convolutional neural network for eeg-based brain-computer interfaces. *Journal of Neural Engineering*, 15(5):056013, 2018. 8
- [28] Hongli Li, Man Ding, Ronghua Zhang, and Chunbo Xiu. Motor imagery eeg classification algorithm based on cnn-lstm feature fusion network. *Biomedical Signal Processing and Control*, 72:103342, 2022. 8, 15
- [29] Yixing Li, Ruobing Xie, Xingwu Sun, Yu Cheng, and Zhanhui Kang. Continuous speech tokenizer in text to speech, 2024. 16
- [30] Ziyue Li, Yuchen Fang, You Li, Kan Ren, Yansen Wang, Xufang Luo, Juanyong Duan, Congrui Huang, Dongsheng Li, and Lili Qiu. Protecting the future: Neonatal seizure detection with spatial-temporal modeling, 2023. 8
- [31] Zhuang Liu, Hanzi Mao, Chao-Yuan Wu, Christoph Feichtenhofer, Trevor Darrell, and Saining Xie. A convnet for the 2020s. In *Proceedings of the IEEE/CVF Conference on Computer Vision and Pattern Recognition (CVPR)*, pages 11976–11986, 2022. 8
- [32] Zechun Liu, Changsheng Zhao, Forrest Iandola, Chen Lai, Yuandong Tian, Igor Fedorov, Yunyang Xiong, Ernie Chang, Yangyang Shi, Raghuraman Krishnamoorthi, Liangzhen Lai, and Vikas Chandra. Mobilellm: Optimizing sub-billion parameter language models for on-device use cases, 2024. 2
- [33] Chao Lou, Zixia Jia, Zilong Zheng, and Kewei Tu. Sparser is faster and less is more: Efficient sparse attention for long-range transformers, 2024. 5
- [34] Zhenyan Lu, Xiang Li, Dongqi Cai, Rongjie Yi, Fangming Liu, Xiwen Zhang, Nicholas D. Lane, and Mengwei Xu. Small language models: Survey, measurements, and insights, 2024. 2
- [35] Sally V Mathias and Meriem Bensalem-Owen. Artifacts that can be misinterpreted as interictal discharges. *Journal of Clinical Neurophysiology*, 36(4):264–274, 2019. 1
- [36] Yuqi Nie, Nam H Nguyen, Phanwadee Sinthong, and Jayant Kalagnanam. A time series is worth 64 words: Long-term forecasting with transformers. In *The Eleventh International Conference on Learning Representations*, 2023. 3
- [37] Iyad Obeid and Joseph Picone. The temple university hospital eeg data corpus. *Frontiers in Neuroscience*, 10:196, 2016. 2, 6, 12
- [38] Damián Pascual, Amir Aminifar, and David Atienza. A self-learning methodology for epileptic seizure detection with minimally-supervised edge labeling. In *2019 Design, Automation & Test in Europe Conference & Exhibition (DATE)*, pages 764–769, 2019. 1
- [39] Wei Yan Peh, Yuanyuan Yao, and Justin Dauwels. Transformer convolutional neural networks for automated artifact detection in scalp eeg, 2022. 8, 15
- [40] Mamunur Rashid, Bifta Sama Bari, and Md. Golam Sadique. Mathematical principals and modeling of EEG signal exploration. *IOSR Journal of VLSI and Signal Processing*, 6(6):05–09, 2016. 1
- [41] Brendan C Reidy, Mohammadreza Mohammadi, Mohammed E Elbity, and Ramtin Zand. Efficient deployment of transformer models on edge TPU accelerators: A real system evaluation. In *Architecture and System Support for Transformer Models (ASSYST @ISCA 2023)*, 2023. 2
- [42] Apple Machine Learning Research. Deploying transformers on the apple neural engine. *Apple Machine Learning Research*, 2022. Published June 6, 2022. 2
- [43] Yannick Roy, Hubert Banville, Isabela Albuquerque, Alexandre Gramfort, Tiago H. Falk, and Jocelyn Faubert. Deep learning-based electroencephalography analysis: a systematic review. *Journal of Neural Engineering*, 16(5):051001, 2019. 1
- [44] Robin Tibor Schirrmeyer, Jost Tobias Springenberg, Lukas Dominique Josef Fiederer, Martin Glasstetter, Katharina Eggensperger, Michael Tangermann, Frank Hutter, Wolfram Burgard, and Tonio Ball. Deep learning with convolutional neural networks for EEG decoding and visualization. *Human Brain Mapping*, 38(11):5391–5420, 2017. 1
- [45] Yonghao Song, Xueyu Jia, Lie Yang, and Longhan Xie. Transformer-based spatial-temporal feature learning for eeg decoding, 2021. 8, 15
- [46] Nathan J Stevenson, Karoliina Tapani, Leena Lauronen, and Sampsa Vanhatalo. A dataset of neonatal eeg recordings with seizure annotations. *Scientific Data*, 6:190039, 2019. 6
- [47] Jen Hong Tan. Pre-training of lightweight vision transformers on small datasets with minimally scaled images, 2024. 5
- [48] Siyi Tang, Jared A. Dunnmon, Liangqiong Qu, Khaled K. Saab, Tina Baykaner, Christopher Lee-Messer, and Daniel L. Rubin. Modeling multivariate biosignals with graph neural networks and structured state space models, 2023. 8
- [49] William O. Tatum, Barbara A. Dworetzky, and Donald L. Schomer. Artifact and recording concepts in EEG. *Journal of Clinical Neurophysiology: Official Publication of the American Electroencephalographic Society*, 28(3):252–263, 2011. 1
- [50] Michal Teplan. Fundamental of eeg measurement. *MEASUREMENT SCIENCE REVIEW*, 2, 2002. 1
- [51] Ashish Vaswani, Noam Shazeer, Niki Parmar, Jakob Uszkoreit, Llion Jones, Aidan N. Gomez, Łukasz Kaiser, and Illia Polosukhin. Attention is all you need. In *Advances in Neural Information Processing Systems*. Curran Associates, Inc., 2017. 3
- [52] Christopher Wang, Vighnesh Subramaniam, Adam Uri Yaari, Gabriel Kreiman, Boris Katz, Ignacio Cases, and Andrei Barbu. BrainBERT: Self-supervised representation learning for intracranial recordings. In *The Eleventh International Conference on Learning Representations*, 2023. 1, 3, 5, 6, 7, 8

- [53] Zhenda Xie, Zheng Zhang, Yue Cao, Yutong Lin, Jianmin Bao, Zhuliang Yao, Qi Dai, and Han Hu. Simmim: A simple framework for masked image modeling, 2022. [3](#), [5](#), [7](#)
- [54] Chaoqi Yang, M. Brandon Westover, and Jimeng Sun. Biot: Cross-data biosignal learning in the wild, 2023. [15](#)
- [55] Zhizhang Yuan, Fanqi Shen, Meng Li, Yuguo Yu, Chenhao Tan, and Yang Yang. Brainwave: A brain signal foundation model for clinical applications, 2024. [1](#)
- [56] Daoze Zhang, Zhizhang Yuan, Yang Yang, Junru Chen, Jingjing Wang, and Yafeng Li. Brant: Foundation model for intracranial neural signal. In *Thirty-seventh Conference on Neural Information Processing Systems*, 2023. [1](#)
- [57] Wei-Long Zheng and Bao-Liang Lu. Investigating critical frequency bands and channels for eeg-based emotion recognition with deep neural networks. *IEEE Transactions on Autonomous Mental Development*, 7(3):162–175, 2015. [6](#)

CEReBrO: Compact Encoder for Representations of Brain Oscillations Using Efficient Alternating Attention

Supplementary Material

A. Experiment Details

A.1. Dataset Pre-processing

This section describes the datasets used in each of our experiments. In Sec. 4.2, Sec. 4.3 and Sec. 4.4 we use TUSL [37], TUSZ [37] and TUEP [37] for pre-training and TUAB for fine-tuning. The smaller pre-training corpus is selected to align with the reduced computational demands of conducting focused ablation studies. In Sec. 4.5, we use TUEG (with the TUAB subset excluded) for pre-training. Note that TUSL, TUSZ and TUEP are subsets of TUEG. We use TUAB, Neonate and SEED for fine-tuning. We incorporate an additional downstream task by fine-tuning CEReBrO on MoBI (see Sec. D). Dataset details can be found in Tab. 8. TUEG contains various channel configurations, illustrated in Fig. 5.

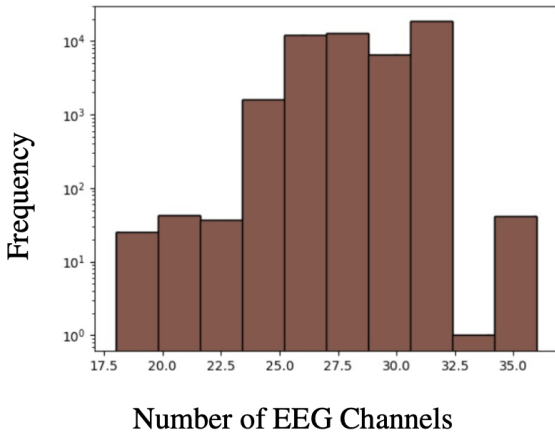


Figure 5. Channel configurations per .edf File in the TUEG Dataset.

A.2. Training Hyperparameters

This section details hyperparameters used to pre-train and fine-tune the models discussed in Sec. 4.5. Our pre-training hyperparameters are available in Tab. 9. Our fine-tuning hyperparameters are available in Tab. 10.

B. Alternatives to Self-Attention

Our tokenization scheme (see Sec. 3.2) generates thousands of tokens per training example. Standard self-attention has quadratic memory and time complexity in the input se-

quence length, which, given our tokenization, limits the potential for deployment in resource-constrained environments. This section discusses the alternatives to self-attention that were explored to address this challenge. We finally selected alternating attention by comparing runtime, memory requirements, and impact on downstream performance (see Algorithm 1).

B.1. Two-Axis Attention

In two-axis attention (Algorithm 2), we compute intra-channel and inter-channel attention in each encoder block using two separate QKV projections. Unlike in alternating attention, each encoder block contributes to learning the spatio-temporal characteristics of the input EEG signals. The primary limitation is that the additional QKV projection in each encoder layer adds more parameters and, therefore, increases the complexity of the model. For example, in CEReBrO Large, two-axis attention yields approximately 20M additional trainable parameters compared to alternating attention.

Algorithm 2 TWO-AXIS ATTENTION

Require: Input tensor \mathbf{T} of shape $[B, C \times N_p, d_e]$

Parameters:

B : batch size

C : number of channels

N_p : number of patches per channel

d_e : embedding dimension

1: **for** each attention block **do**

2: Compute projections: Q_c, K_c, V_c and Q_p, K_p, V_p

3: Reshape \mathbf{T} to $[B \times N_p, C, d_e]$

4: $\mathbf{A}_1 =$ Multi-head attention over channels using (Q_c, K_c, V_c)

5: Reshape \mathbf{T} to $[B \times C, N_p, d_e]$

6: $\mathbf{A}_2 =$ Multi-head attention over patches using (Q_p, K_p, V_p)

7: Reshape \mathbf{A}_1 and \mathbf{A}_2 back to $[B, C, N_p, d_e]$

8: Compute $\text{Mean}(\mathbf{A}_1, \mathbf{A}_2)$ ▷ Combine outputs

9: **end for**

Ensure: Output tensor of shape $[B, C \times N_p, d_e]$

B.2. Bottleneck Attention

Bottleneck attention expands upon two-axis attention, intending to have intra-channel and inter-channel attention computation in each encoder block without resorting to two separate QKV projections. The idea is first to compute

Dataset	# Samples	# Channels	Sample Duration (s)	Sampling Frequency (Hz)
TUEP	303,081	23	5	256
TUSL	16,503	23	5	256
TUSZ	598,944	23	5	256
TUAB	819,561	23	5	256
Neonate	80,536	19	5	256
MoBI	542,444	60	2	100
SEED	152,730	62	1	200
TUEG (w/o TUAB subjects)	15,783,482	18-36	5	256

Table 8. Dataset details.

	CEReBrO Small	CEReBrO Base	CEReBrO Large
Batch Size		4096	
Scheduler		Cosine + Linear warmup	
Optimizer		AdamW	
Betas		[0.9, 0.98]	
Peak learning rate		1.25e-3	
Minimum learning rate		2.5e-7	
Maximum allowed epochs		100	
Training stopped at epoch		30	
Warmup epochs		3	
Masking ratio		0.5	
Encoder layers	8	10	12
Number of attention heads per layer		12	
Embedding dimension	192	576	768
MLP Size	768	2304	3072
Weight decay		0.05	
Patch size		64	

Table 9. Pre-training hyperparameters. The same hyperparameters are used across all model sizes, with a few exceptions specified in this table.

inter-channel attention and use the resulting attention map as a value vector in the intra-channel attention computation. Details are discussed in Algorithm 3.

B.3. Theoretical and Empirical Complexity Analysis of Different Attention Mechanisms

In Fig. 6, we plot runtime and GPU memory consumption of our different attention mechanisms as functions of input sequence lengths. Several key patterns emerge. First, it is clear that two-axis, bottleneck, and alternating attention all require less memory (up to $5\times$ less) and have quicker runtimes (more than $2\times$ faster) than standard self-attention. Bottleneck attention and alternating attention have very similar memory and runtime profiles. The benefits of bot-

tleneck, two-axis, and alternating attention are highlighted for large sequence lengths. Our findings in Tab. 12 corroborate this, which suggests that the true benefit emerges when $C + N_p \ll CN_p$.

B.4. Performance Comparisons for Different Attention Mechanisms

In Tab. 12, we observe distinct spectrogram results compared to waveforms. Standard self-attention yields the most competitive results across all three spectrogram metrics, closely followed by two-axis and alternating attention. In contrast, two-axis and alternating attention outperform standard self-attention for waveforms. In both regimes, bottleneck split attention is considerably worse than standard self-

	CEReBrO Small	CEReBrO Base	CEReBrO Large
Batch Size		4096	
Scheduler		Cosine + Linear warmup	
Optimizer		AdamW	
Betas		[0.9, 0.999]	
Peak learning rate		5e-4	
Minimum learning rate		2.5e-7	
Total epochs		50	
Warmup epochs		5	
Layer-wise learning rate decay factor		0.75	
Weight decay		0.05	
Gaussian noise amplitude ratio		0.2	
Gaussian noise addition probability		0.5	
Drop path	0.1	0.2	0.2
Label smoothing		0.1	

Table 10. Fine-tuning hyperparameters. The same fine-tuning hyperparameters are used for all three model sizes, with a few exceptions specified in this table.

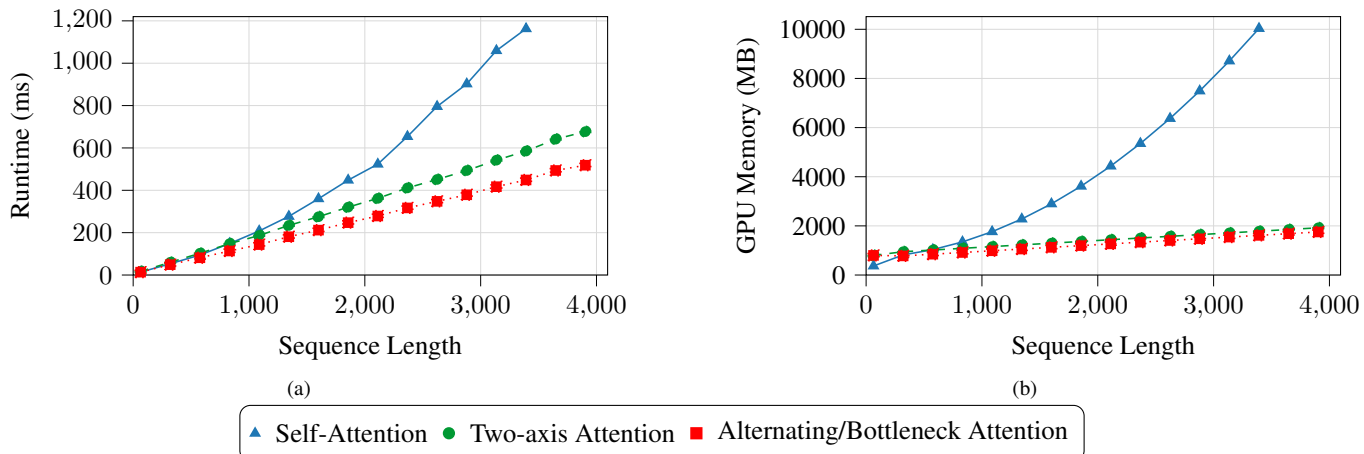


Figure 6. (a) Runtime vs input sequence length for different attention mechanisms. (b) GPU memory usage vs. input sequence length for different attention mechanisms. In these experiments we use CEReBrO Large on 4 NVIDIA RTX 2080 Ti GPUs. We use $N_p = 20$ and $C \in [1, 64]$ to replicate typical EEG configurations. For self-attention, we run out of GPU memory for sequence lengths larger than 3392.

Attention Type	Memory Complexity	Time Complexity
Alternating (over p)	$\mathcal{O}(CN_p^2)$	$\mathcal{O}(CN_p^2d_e)$
Alternating (over C)	$\mathcal{O}(C^2N_p)$	$\mathcal{O}(C^2N_pd_e)$
Bottleneck	$\mathcal{O}(CN_p(C + N_p))$	$\mathcal{O}(CN_p(C + N_p)d_e)$
Two-Axis	$\mathcal{O}(CN_p(C + N_p))$	$\mathcal{O}(CN_p(C + N_p)d_e)$
Standard	$\mathcal{O}((CN_p)^2)$	$\mathcal{O}((CN_p)^2d_e)$

Table 11. Theoretical memory and time complexities of each attention mechanism.

attention. We also observe that the best waveform representation yields significant improvements (notably +1.75% in the balanced accuracy, +0.0182 in the AUPR and +0.0135 in the AUROC) compared to the best spectrogram representation. A waveform representation yields better performance across all metrics than a spectrogram representation. Based on these results, our final model (presented in Sec. 3 and Sec. 4) uses waveform representations of EEG signals and alternating attention. This combination yields the best balance between efficiency (as presented in Fig. 6) and performance (as presented in Tab. 12).

Algorithm 3 BOTTLENECK SPLIT ATTENTION

Require: Input tensor \mathbf{T} of shape $[B, C \times N_p, d_e]$

Parameters:

B : batch size

C : number of channels

N_p : number of patches per channel

d_e : embedding dimension

- 1: **for** each attention block **do**
- 2: Compute QKV projections: Q, K, V of shape $[B, C, N_p, d_e]$
- 3: Compute $(Q, K, V)_{\text{avg}(N_p)} = \text{MeanPool}(Q, K, V)$ over N_p , resulting in shape $[B, C, 1, d_e]$
- 4: $\mathbf{A}_1 = \text{Attention}(Q_{\text{avg}(N_p)}, K_{\text{avg}(N_p)}, V_{\text{avg}(N_p)})$
- 5: Compute $(Q, K)_{\text{avg}(C)} = \text{MeanPool}(Q, K)$ over C , resulting in shape $[B, 1, N_p, d_e]$
- 6: Broadcast \mathbf{A}_1 to shape $[B, C, N_p, d_e]$
- 7: Compute Attention($Q_{\text{avg}(C)}, K_{\text{avg}(C)}, \mathbf{A}_1$)
- 8: **end for**

Ensure: Output tensor of shape $[B, C \times N_p, d_e]$

Representation	Attention	Balanced Accuracy (%)	AUPR	AUROC
Spectrogram	Bottleneck	77.49	0.8548	0.8545
	Alternating	78.49	0.8684	0.8674
	Two-Axis	78.83	0.8702	0.8671
	Standard	78.89	0.8719	0.8690
Waveform	Bottleneck	78.20	0.8640	0.8594
	Standard	79.35	0.8755	0.8700
	Two-Axis	80.57	0.8885	0.8820
	Alternating	80.65	0.8901	0.8825

Table 12. The effect of each attention mechanism in pre-training and fine-tuning on anomaly classification.

C. Incorporating Magnitude and Phase Information Into Spectrogram Tokenization

In Tab. 13, we study the impact of combining magnitude and phase information when spectrograms are used as input to our model. Specifically, we introduce phases as additional "channels" in our spectrogram tensors, and we evaluate the resulting performance on the TUAB dataset.

We follow two approaches to introduce the phase: the interleaved approach and the separated approach.

In the interleaved approach, we construct the channels as

$$[\text{magnitude}_1, \text{phase}_1, \text{magnitude}_2, \text{phase}_2, \dots, \text{magnitude}_C, \text{phase}_C] \quad (4)$$

where magnitude_i and $\text{phase}_i, i \in [1, 23]$ represent the pre-processed magnitude and phase tensors of channel i .

In the separated approach, we construct the channels as

$$[\text{magnitude}_1, \text{magnitude}_2, \dots, \text{magnitude}_{23}, \text{phase}_1, \text{phase}_2, \dots, \text{phase}_{23}] \quad (5)$$

Including phase information doubles the number of tokens in each training example, and we aim to evaluate if

this addition results in an increased accuracy.

Tab. 13 illustrates the performance of CEReBrO Large trained from scratch on TUAB with and without phase information. No statistical evidence suggests that including phase information, whether in the interleaved or separated regime, yields a performance improvement.

Spectrogram Information	Balanced Accuracy (%)
Magnitude only	77.01
Magnitude + interleaved phase	76.01
Magnitude + separated phase	76.89

Table 13. Comparison of spectrogram magnitude vs. magnitude and phase information on anomaly classification.

D. Additional Downstream Tasks

In this section, we provide additional downstream tasks. In particular, we use the MoBI dataset [17]. Mobile brain-body imaging data is collected during a treadmill-based BCI task involving lower limb motor imagery. Six goniometers recorded bilateral joint angles (hip, knee, and ankle), aiming to regress 12 targets (left and right leg angles). Data were gathered from 8 healthy subjects, each completing three identical trials. During fine-tuning, we use an MSE loss function and report R^2 and RMSE scores as performance metrics. Results are included in Tab. 14.

Methods	Model Size	R^2 Score	RMSE
Supervised Models			
SPaRCNet [23]	0.79M	0.1467 ± 0.0064	0.1344 ± 0.0006
CNN-Transformer [39]	3.2M	0.0628 ± 0.0089	0.1411 ± 0.0007
FFCL [28]	2.4M	0.0712 ± 0.0124	0.1396 ± 0.0014
ST-Transformer [45]	3.5M	0.2911 ± 0.0014	0.1222 ± 0.0001
Self-supervised Models			
BIOT [54]	3.2M	0.0597 ± 0.0069	0.1401 ± 0.0006
LaBraM-Base [21]	5.8M	0.2876 ± 0.0032	0.1225 ± 0.0003
LaBraM-Large [21]	46M	0.3093 ± 0.0032	0.1197 ± 0.0003
LaBraM-Huge [21]	369M	0.3145 ± 0.0032	0.1196 ± 0.0003
CEReBrO	3.58M	0.1036 ± 0.0007	0.1375 ± 0.0005
CEReBrO	39.95M	0.2776 ± 0.0002	0.1239 ± 0.0006
CEReBrO	85.15M	0.3118 ± 0.0032	0.1209 ± 0.0004

Table 14. Performance on gait prediction using MoBI.

In Tab. 14, we see that CEReBrO Large surpasses LaBraM Large and LaBraM base in the R^2 score while yielding comparable RMSE. However, it performs slightly worse than LaBraM Huge, which is $4\times$ larger. Overall, even in a regression task, we see that CEReBrO remains competitive compared to the current state of the art.

E. Comparing LaBraM and CEReBrO

LaBraM yields competitive results at all model sizes, frequently surpassing CEReBrO. However, we posit that

several aspects of LaBraM make it challenging to train and deploy in resource-constrained environments. Firstly, LaBraM requires multi-stage pre-training: a discrete neural tokenizer has to be pre-trained, followed by the LaBraM encoder. This increases LaBraM’s memory footprint and pre-training time, making LaBraM less flexible in the face of distribution shifts downstream. LaBraM’s discrete neural tokenizer also has limitations. For example, codebook size selection is non-trivial and highly depends on the characteristics of the input data. Secondly, discrete codebooks have been shown to suffer from information loss [29]. LaBraM’s encoder uses standard self-attention, which may capture more correlations in the data, but is also more memory-intensive and slower than alternating attention, especially for larger sequence lengths. In Tab. 15, we illustrate the peak memory usage of LaBraM and CEReBrO. While the memory usage is comparable, these values do not include the non-trivial memory usage of LaBraM’s neural tokenizer, especially during pre-training.

Model	Model Size	Peak GPU Memory Usage (MB)
LaBraM	5.8M	757.38
	46M	1371.92
	369M	2758.42
CEReBrO	3.58M	402.96
	39.95M	1016.31
	85.15M	1620.29

Table 15. Comparison of Peak GPU Memory Usage for the best performing LaBraM and CEReBrO models. In each model, we use $C = 64$ and batch size = 8.